catalysts

MDPI

Article

Magnetic TiO_2/Fe_3O_4-Chitosan Beads: A Highly Efficient and Reusable Catalyst for Photo-Electro-Fenton Process

Soumaya Rezgui [1,2,*], Aida M. Díez [1], Lotfi Monser [2], Nafaa Adhoum [2], Marta Pazos [1] and M. Ángeles Sanromán [1]

[1] BIOSUV Research Group, INTECX Building, University of Vigo, Lagoas-Marcosende Campus, 36310 Vigo, Spain
[2] Research Unit in Electrochemistry, Materials and Environment (UR16ES02), IPEIK, University of Kairouan, Kairouan 3100, Tunisia
* Correspondence: soumaya.rezgui@insat.rnu.tn

Abstract: Heterogeneous photo-electro-Fenton process is an attractive technology for the removal of recalcitrant pollutants. To better exploit the presence of an irradiation source, a bifunctional catalyst with TiO_2 nanoparticles embedded into an iron–chitosan matrix was developed. The catalytic activity of the catalyst was improved by the optimization of the loaded TiO_2content. The prepared composite catalysts based on TiO_2, Fe_3O_4 and chitosan were called TiO_2/Fe_3O_4-CS beads. The best catalyst with an optimal ratio TiO_2/Fe = 2 exhibited a high efficiency inthe degradation and mineralization of chlordimeform (CDM) insecticide. Under the optimum conditions (concentration of catalyst equal to 1 g L^{-1} and applied current intensity equal to 70 mA), a real effluent doped with 30 mg L^{-1} of CDM was efficiently treated, leading to 80.8 ± 1.9% TOC reduction after 6 h of treatment, with total removal of CDM after only 1 h.The generated carboxylic acids and minerals wereidentified and quantified. Furthermore, the stability and reusability of the developed catalyst was examined, and an insignificant reduction in catalytic activity was noticed forfour consecutive cycles of the photo-electro-Fenton process. Analyses using SEM, XRD and VSM showed a good stability of the physicochemical properties of the catalyst after use.

Keywords: photo-electro-Fenton process; chlordimeform; wastewater treatment; bifunctional catalyst

Citation: Rezgui, S.; Díez, A.M.; Monser, L.; Adhoum, N.; Pazos, M.; Sanromán, M.Á. Magnetic TiO_2/Fe_3O_4-Chitosan Beads: A Highly Efficient and Reusable Catalyst for Photo-Electro-Fenton Process. *Catalysts* **2022**, *12*, 1425. https://doi.org/10.3390/catal12111425

Academic Editors: Jorge Bedia and Carolina Belver

Received: 16 October 2022
Accepted: 9 November 2022
Published: 13 November 2022

1. Introduction

In recent decades, the extensive use of pesticides to improve agricultural production has led to an increased risk of water pollution. In fact, these pollutants can be classified as persistent and extremely toxic organic substances. The ability of these harmful pollutants to easily bioaccumulate even at very low concentrations represents a serious issue that can cause problems for the environment, human health and living organisms [1]. Consequently, the removal of pesticides from water and wastewater has become a great global challenge.

In recent years, electrochemical advanced oxidation processes (EAOPs) have been-considered an option for the removal of toxic and persistent organic micropollutants from wastewater [2–4]. One of the most powerful and attractive techniques among EAOPs is the electro-Fenton (EF) process, where by hydrogen peroxide (H_2O_2) is generated at a cathode by O_2 reduction (Equation (1)), and a ferrous ion or iron oxide catalyst is added to the effluent [5]. The EF process is very effective in the mineralization of organic pollutants due to the production of strongly oxidizing hydroxyl radicals through the Fenton reaction (Equation (2)) [6]. However, this technology is limited by a few factors, such as the rapid accumulation of Fe(III) ions and the possibility of their complexation with hydroxyl ions and oxidation products during treatment [7].

$$O_2 + 2\,H^+ + 2\,é \rightarrow H_2O_2 \quad (1)$$

$$H_2O_2 + Fe^{2+} \rightarrow Fe^{3+} + OH^- + \bullet OH \quad (2)$$

The presence of UV irradiation has two specific aims: the regeneration of Fe(II) ions and the degradation of the formed complexes until their mineralization due to an additional production of •OH [8]. This process is called the photo-electro-Fenton (PEF) process, and it leads to great performance in the mineralization of organic pollutants [9,10].

However, the application of UV irradiation could increase the operational cost, but it can be justified by the use of a photocatalyst, such as TiO_2, to increase its economic costeffectiveness. The application of a ferromagnetic-TiO_2 composite material is widely used for photocatalysis due to its efficiency and magnetic properties [11,12].

In fact, in a heterogeneous system, many solid catalysts containing iron, such as Fe, Fe_2O_3, Fe_3O_4 and FeOOH, were successfully used for the treatment of recalcitrant organic pollutants in water [13–17]. Among iron oxides, the immense popularity of Fe_3O_4 as a catalyst originates from its broad application potential due to high saturation magnetization, easy handling, relatively low cost, non-toxicity and environmentally friendly character [18,19]. Titanium oxide (TiO_2) has also shown widespread photocatalytic application in the field of wastewater treatment due to its unrivalled properties of non-toxicity, easy UV activation, chemical stability and availability [20]. Despite all these outstanding properties, TiO_2 deployment for photocatalytic application has witnessed drawbacks due to its large energy band gap of about 3.2 eV [20,21]. In addition, one of the problems hindering TiO_2 use is its agglomeration in aqueous solution, which requires a post-filtration treatment [21]. In order to overcome the problem of the band gap of TiO_2, several studies revealed that the presence of Fe_3O_4 enhances the photocatalytic activity of TiO_2 by decreasing the charge carrier recombination, with a band gap of the composite material around 2.5 eV. This is caused by the generated Z-scheme on the composite TiO_2/Fe_3O_4 where the recombination between holes and electrons on TiO_2 is restrained by the addition of another valence band (Fe_3O_4). Indeed, Fe-species have been reported as an outstanding alternative for creating Z-scheme photocatalytic heterojunction systems [22]. Moreover, this modified TiO_2 nanoparticle can be separated from water by means of an external magnetic field [11,23]. However, the use of magnetic separation is complicated in real water applications. Therefore, the use of a catalytic support, such as chitosan, for both metal oxides (Fe_3O_4 and TiO_2) not only avoids the agglomeration issue, but it also facilitates catalyst recovery, protects ferroparticles from oxidation and extends their storage life [24].

Therefore, in the present study, we innovatively synthesized the TiO_2/Fe_3O_4-CS catalytic beads through a green co-precipitation method in only one step. The co-precipitation method involves the dispersal of a mixture of chitosan and metals into an alkaline solution to form nanoparticles strongly bound to chitosan with attractive catalytic and magnetic properties for easy catalyst recovery and reuse [24–28]. TiO_2/Fe_3O_4-CS was used as a novel nano-structured heterogeneous catalyst for the oxidation of CDM insecticide by an efficient cyclic PEF process; therefore, Fe(II), within the structure of Fe_3O_4, can activate the Fenton system [29], and TiO_2 acts as a photocatalyst to better exploit the use of UV irradiation. In the PEF system, an electrochemical reactor was used for the electrogeneration of H_2O_2, and the catalyst was added to a second photocatalytic reactor. The effects of operational parameters were studied, such as the TiO_2 loading in the beads, catalyst dosage and the current intensity applied. Under optimal conditions, aqueous wastewater doped with 30 mg L^{-1} of CDM was treated. The carboxylic acids and inorganic ions generated during the treatment process were identified and quantified. Finally, the electric energy consumed was estimated, and the stability of the best catalyst in terms of CDM and TOC removal efficiencies was studied.

2. Results

2.1. Optimization of Operational Parameters

2.1.1. Performance Comparison of Several Processes for the Removal of CDM

Initially, some control experiments were performed. To begin with, the adsorption assays of the developed catalytic beads showed no CDM adsorption after 4 h of treat-

ment on the synthesized catalytic beads (data not shown). Then, the low efficiencies of photoelectrolysis–H_2O_2 (electrogenerated H_2O_2 + UV-LED) and photocatalysis (1 g of TiO_2/Fe_3O_4-CS catalyst + UV-LED) systems revealed, respectively, 70.6 ± 5.3% and 13.2 ± 4.4% of CDM removal yield after 1 h of electrolysis (Figure 1) along with only 18.2 ± 3.3% and 4.4 ± 1.6% of TOC abatement after 4 h of treatment (Table 1). However, the PEF process running at I = 50 mA and pH_i = 3, in the presence of 1 g L^{-1} TiO_2/Fe_3O_4-CS, exhibited higher efficiency, with total degradation of CDM after only 1 h and TOC abatement equal to 69.6 ± 2.7% after 4 h of treatment (Table 1).

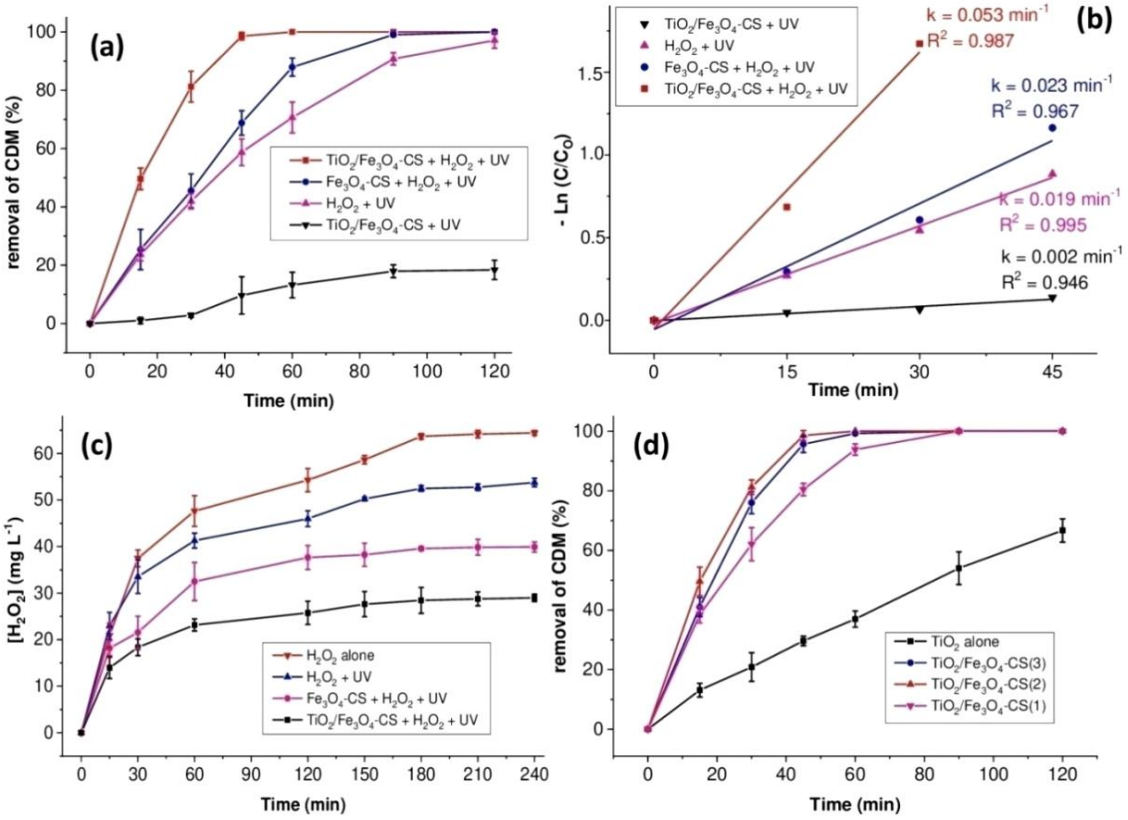

Figure 1. Performance comparison of several processes and effect of the addition of TiO_2 to magnetic chitosan beads: (**a**,**d**) % removal of CDM; (**b**) −Ln (C/C0) vs. time; (**c**) [H_2O_2] vs. time: I = 50 mA in the presence of 1 g L^{-1} of catalyst and at pH_i = 3.

2.1.2. Influence of TiO_2 in Magnetic Chitosan Beads

As found previously in the PEF system, the composite catalyst TiO_2/Fe_3O_4-CS showed higher catalytic activity, with total degradation of CDM after only 1 h and TOC abatement of around 70% after 4 h of treatment. However, in the presence of Fe_3O_4-CS catalytic beads, only 87.9 ± 3.1% CDM removal yield and TOC abatement was achieved, not exceeding 33.9 ± 4.1%. The higher photocatalytic activity of TiO_2/Fe_3O_4-CS beads could be attributed to the acceleration of electron mobility in the $Fe^{III/II}/TiO_2$ system [12,30] and the synergistic combination of PEF with photocatalysis. It is widely reported that the combination of TiO_2 and Fe_3O_4, with their different band gaps, can suppress the electron–hole recombination, enhancing the photocatalytic activity, and thus, the PEF process efficiency, thanks to the generation of the Z-scheme [11,22,30–32]. Moreover, the degradation of CDM by the PEF process was found to follow a pseudo-first-order kinetic (Figure 1b), which is probably related to the steady •OH concentration throughout the treatment process [33,34]. To evaluate the catalytic decomposition of the oxidant, the concentration of H_2O_2 was monitored during treatment with and without the developed catalysts, and the results are presented in Figure 1c. In the absence of the catalyst and UV-LED lamp, the accumulated amount of H_2O_2 after 4 h of electrolysis was estimated

at 64.4 ± 0.5 mg L^{-1}. In the presence of UV-LED irradiation, the concentration of H_2O_2 decreased to 53.8 ± 0.9 mg L^{-1}, which means that the amount of H_2O_2 decomposed by photolysis after 4 h of electrolysis was around 16.6%. As expected, by adding the Fe_3O_4-CS and TiO_2/Fe_3O_4-CS catalytic beads to the (H_2O_2 + UV-LED) system, the concentration of the oxidant decreased significantly to 39.9 ± 1.1 mg L^{-1} and 29 ± 0.8 mg L^{-1}, respectively, indicating that approximately 38% and 55% of the H_2O_2 amount was decomposed. These findings were in agreement with our previous results, and they confirmed the best catalytic activity of TiO_2/Fe_3O_4-CS beads because an increase in the decomposition rate of H_2O_2 is related to an increase in the production yield of •OH radicals [35]. Therefore, it is clear that the incorporation of TiO_2 into magnetic CS beads favors an effective usage of H_2O_2, allowing great improvement to the PEF process efficiency.

Table 1. Summary table of mineralization rates.

Parameter	Assay	Rate of TOC Removal after 4 h of Treatment
Performance comparison of several processes	TiO_2/Fe_3O_4-CS(2) + UV-LED	4.4 ± 1.6
	H_2O_2 + UV-LED (Without catalyst)	18.2 ± 3.3
	TiO_2/Fe_3O_4-CS(2) + H_2O_2 + UV-LED	69.6 ± 2.7
Influence of TiO_2 in magnetic chitosan beads	Fe_3O_4-CS + H_2O_2 + UV-LED	33.9 ± 4.1
	TiO_2/Fe_3O_4-CS(2) + H_2O_2 + UV-LED	69.6 ± 2.7
Effect of TiO_2 loading content into magnetic chitosan beads	Molar ratio TiO_2/Fe = 1	38.2 ± 3.5
	Molar ratio TiO_2/Fe = 2	69.6 ± 2.7
	Molar ratio TiO_2/Fe = 3	54.2 ± 5.6
	Catalytic beads of TiO_2	24.5 ± 1.9
Effect of catalyst dosage	0.25 g L^{-1}	40.9 ± 4.1
	0. 5 g L^{-1}	60.8 ± 3.2
	1 gL^{-1}	69.6 ± 2.7
	1.5 g L^{-1}	70.2 ± 1.7
	2 g L^{-1}	58.2 ± 6.2
Effect of current intensity	50 mA	68.6 ± 4.9
	70 mA	76.9 ± 3.7
	100 mA	77.7 ± 1.2

2.1.3. Effect of TiO_2 Loading Content into Chitosan Beads

In order to increase the catalytic activity of TiO_2/Fe_3O_4-CS beads, the effect of TiO_2 content in the catalyst was studied. For this purpose, the molar ratio TiO_2/Fe was varied during the preparation of the catalyst from 1 to 3 (to facilitate a designation of the developed catalysts, the molar ratio values between the brackets were added to TiO_2/Fe_3O_4-CS). The results showed that a molar ratio equal to 2 (TiO_2/Fe_3O_4-CS(2)) was optimal, leading to total degradation of CDM after 1 h (Figure 1d) and TOC removal yield of around 70% after 4 h of treatment (Table 1), against 38.2 ± 3.5% and 54.2 ± 5.6%, respectively, for the molar ratios TiO_2/Fe = 1 and 3. On the other hand, the comparison of the photocatalytic activities of TiO_2/Fe_3O_4-CS(2) and TiO_2-CS (Figure 1d) showed a remarkable difference in their catalytic performance, which was greater for the composite catalyst. In fact, the CDM degradation rate did not exceed 35% after 1 h of treatment using TiO_2-CS beads, with low TOC abatement estimated at 24.5 ± 1.9% after 4 h of treatment. Therefore, it is obvious that the Fe(II) ions in TiO_2/Fe_3O_4-CS catalytic beads notably improve their catalytic performance by the Fenton reaction with H_2O_2, so that •OH radicals are produced. Numerous studies have reported the high photocatalytic activity of the mixture of TiO_2/Fe_3O_4 compared to pure TiO_2, and they explained this improvement by the fast photogenerated electron transfer between Fe_3O_4 and TiO_2, which can effectively reduce electron/hole recombination [12,33,36,37].

To sum up, a molar ratio TiO_2/Fe = 2 is optimal both for the removal of the pollutant and its mineralization. In fact, varying the molar ratio from 1 to 2, the photocatalytic activity of the catalytic beads increased through the increase in TiO_2 active sites. The improvement in pollutant degradation and mineralization by the increase in TiO_2 load in

the iron catalysts has already been reported by many research studies, and it is related to the enhancement of the electron transfer reducing electron–hole recombination [32,38]. For a molar ratio TiO_2/Fe = 3, the catalytic performance of the system decreased due to the decrease in active iron sites in favor of the photocatalytic sites of TiO_2, which has a wide band gap energy, causing a rapid recombination of the electron–hole pairs [39]. It is well known that the fast recombination of charge carriers significantly lowers the photocatalytic performance [24,40]. Thus, a TiO_2/Fe molar ratio equal to 2 was optimal for the preparation of TiO_2/Fe_3O_4-CS beads, and the catalyst TiO_2/Fe_3O_4-CS(2) was selected thereafter.

The photodegradation of pesticides using TiO_2/Fe_3O_4-based materials as catalysts has been poorly reported. Compared to the efficiency of TiO_2/Fe_3O_4 composite catalysts listed in Table 2, TiO_2/Fe_3O_4-CS showed good catalytic activity. Nevertheless, the reactor set-up, such as the irradiation source, can greatly affect the overall efficiency of the process [41].

Table 2. The comparison of photodegradation efficiency of TiO_2/Fe_3O_4-CS catalytic beads with other TiO_2/Fe_3O_4-based materials against different pesticides.

Catalysts	Pesticides	Degradation Efficiency (%)	Refs.
Fe_3O_4-TiO_2/reduced graphene oxide	Atrazine	99% within 40 min	[42]
N-doped TiO_2@SiO_2@Fe_3O_4 nanocomposite	Paraquat	98.7% within 180 min	[43]
Bare 3D-TiO_2/magnetic biochar dots	Diazinon	98.5% within 30 min	[44]
TiO_2/Fe_3O_4-CS	Chlordimeform	100% removal within 60 min	Present work

2.1.4. Effect of Catalyst Dosage

Catalyst dosage was another parameter affecting the heterogeneous Fenton reaction [45]. The effect of catalyst dosage on the degradation of CDM by the PEF process was studied by applying a current intensity of 50 mA at $pH_{initial}$ = 3. It is clear from Figure 2a that the increase in TiO_2/Fe_3O_4-CS(2) catalytic beads from 0.25 g L^{-1} to 1 g L^{-1} increased the rate of CDM removal, and an almost total degradation was obtained for all assays after 1 h of treatment, with an improvement in TOC abatement, respectively, from 40.9 ± 4.1% to 69.6 ± 2.7% (Table 1). For a concentration equal to 1.5 g L^{-1}, there was a trivial enhancement in CDM and TOC removal efficiencies. However, the removal yields of CDM and TOC were decreased for a high concentration equal to 2 g L^{-1}. Indeed, an increase in the concentration of catalytic beads in solution can inhibit the penetration of light into the photocatalytic reactor [46,47]. Additionally, an increase in the active catalytic sites can cause secondary reactions with •OH radicals, thus producing less reactive oxidizing species (Equation (3)), which can reduce the efficiency of the process for the mineralization of organic pollutants [25].

$$Fe^{2+} + \bullet OH \rightarrow Fe^{3+} + OH^- \quad (3)$$

2.1.5. Effect of the Current Intensity

The current intensity applied is a key parameter in the electrochemical Fenton technologies because it is the driving force for the reduction in oxygen, leading to the generation of H_2O_2 at the cathode, and it affects the regeneration of Fe(II) [48]. In order to study the effect of the current intensity applied on CDM degradation and its mineralization by the PEF process, several experiments were carried out using different current intensities in the range from 50 mA to 100 mA in the presence of 1 g of TiO_2/Fe_3O_4-CS(2) and at initial acid pH (Figure 2b). The results showed that an increase in the current intensity from 50 mA to 70 mA leads to total degradation of the pollutant after only 1 h, with almost 10% improvement in TOC abatement (Table 1). This finding can be mainly attributed to the fast production of H_2O_2 at a higher current and the fast regeneration of Fe(II) enhancing the production of •OH radicals [49].

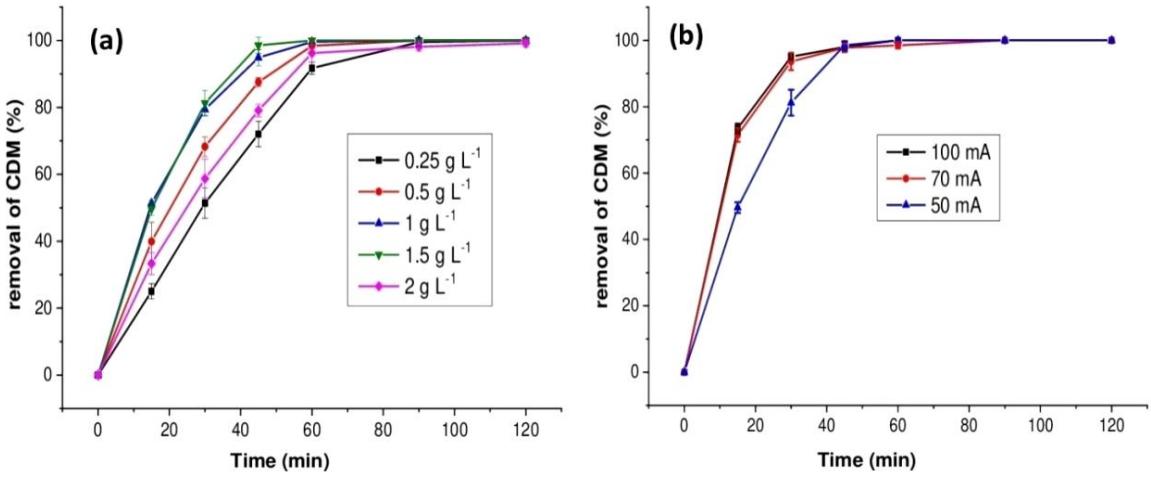

Figure 2. (**a**) Effect of catalyst dosage, (**b**) Effect of current intensity.

As seen in Figure 2b and Table 1, no further increase in the removal efficiencies was observed for the current intensity applied beyond 70 mA. This behavior can indicate that parasitic reactions, such as the four-electron reduction in O_2 with H_2O formation, as well as the decomposition and hydrogenation of H_2O_2, would take place when the current increased beyond a certain value [49–52]. On the other hand, working at higher current intensities can generate a degradation of our organic catalytic support "CS". In fact, several studies have shown the degradation of CS in the presence of an irradiation source and high concentrations of H_2O_2 [53,54]. An optimal current intensity equal to 70 mA, which ensured high treatment efficiency and good catalyst stability, was therefore established for the upcoming experiments.

To confirm the role of •OH radicals in the mineralization of the organic pollutant, isopropanol was used as a •OH scavenger. The degradation of CDM was totally inhibited in the presence of isopropanol. Thus, •OH should be the main active species for the degradation of CDM by the PEF process.

2.2. Treatment of Wastewater Doped with Chlordimeform by Photo-Electro-Fenton Process

To evaluate the applicability of the PEF process using TiO_2/Fe_3O_4-CS(2) as a catalyst for the removal of CDM in a more complex matrix than ultrapure water, an experiment was carried out on secondary treated wastewater kindly given by the municipal wastewater treatment plant in the northwest of Spain, whose physiochemical characteristics are summarized in Table 3.

Table 3. Physicochemical properties of the collected wastewater.

Parameter	Value
Total organic carbon TOC (mg L^{-1})	52.7
Chemical oxygen demand DCO (mg L^{-1})	35
Biological oxygen demand BOD_5 (mg L^{-1})	2
Conductivity (mS cm^{-1})	3.33
pH	7.31
Turbidity (mg L^{-1})	12

Under optimal experimental conditions ($[CDM]_i$ = 30 mg L^{-1}, $[TiO_2/Fe_3O_4$-CS(2)] = 1 g L^{-1}, and I = 70 mA), total degradation of CDM was achieved after 1 h, and TOC abatement reached 50.6 ± 5.1% after 1 h of electrolysis; then, it increased slowly to attain 80.8 ± 1.9% after 6 h of treatment (Figure 3b).

Furthermore, a slight decrease in the efficiency of the system was noticed compared to previous results when ultrapure water was used as the matrix (Figure 2b). This finding

can be explained, according to zazouli et al. [55], by the presence of organic matter and inorganic anions in wastewater. In fact, the anions (X^-) can react with the •OH to produce $X^{-\bullet}$ radicals, which are less reactive.

In addition to the aqueous matrix influence, it should be noted that EEC is another big concern, which should be considered for sustainable development [56]. The results showed that global EEC was low compared to some literature values on the treatment of real wastewater by electrochemical processes [57–59] around 1.7 kWh m^{-3} and 1.4 kWh m^{-3}, respectively, for real wastewater and ultrapure water matrices. However, it should be noted that the difference (≃0.3 kWh m^{-3}) is probably due to the presence of degradable compounds in the treated wastewater matrix, whose oxidation requires a little more energy.

2.3. Evaluation of Organic Acids and Minerals Produced during Treatment

Studies of organic pollutants' mineralization by advanced oxidation processes show that oxidation by •OH radicals leads to the formation of carboxylic acids [60,61]. To better assess the oxidative capacity of our PEF process, an analysis of carboxylic acids was performed in order to identify and quantify them during treatment. The evolution of the identified acids during the mineralization of CDM is presented in Figure 3c. All the acids produced reached their maximum concentrations after around 2 h. Then, they decreased to a zero value after 6 h of treatment, indicating the deep mineralization of all detected acids. The concentration of oxalic acid during the treatment process was low (almost zero), which can be explained by the high reactivity of oxalic acid with Fe(III) and the formation of Fe(III)–oxalate complexes that are easily photolysed in the presence of UV light and H_2O_2 oxidant [62]. However, the other acids detected were malonic, succinic, formic and glycolic acids, appearing at the beginning of treatment. These results showed the effectiveness of our PEF process in removing the aliphatic compounds known for their resistance to oxidation.

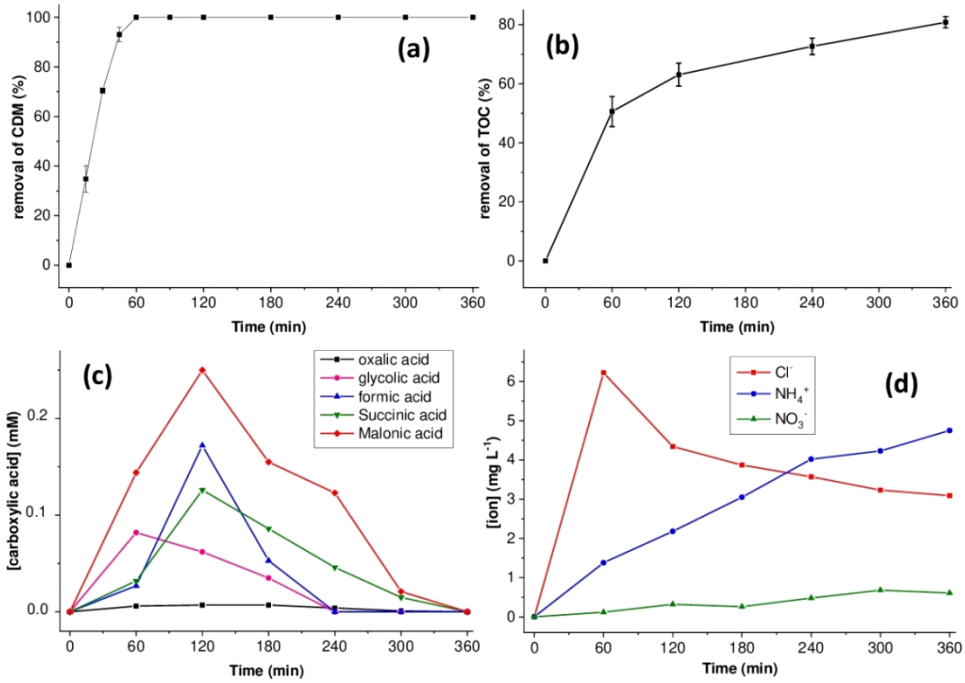

Figure 3. Treatment of a real effluent: (**a**) % removal of CDM; (**b**) % removal of TOC; (**c**) [carboxylic acids] vs. time (**d**) [ions] vs. time: I = 70 mA in the presence of 1 g L^{-1} of TiO_2/Fe_3O_4-CS(2) and at $pH_{initial}$ = 3.

On the other hand, considering the CDM molecule is composed of a chlorine atom and two nitrogen atoms, its treatment by an advanced oxidation process leads to the production of minerals. The evolution of these ions was monitored by ion chromatography. The ob-

tained results (Figure 3d) showed that the chloride ions reached a maximum concentration of 6.22 mg L^{-1} after 1 h; this concentration presented the total amount initially present in the parent molecule. This finding was in agreement with several studies, which have shown that the release of chloride ions is rapid using a BDD anode and that the dechlorination of aromatic compounds occurs before the opening reaction of the aromatic cycle [63–65]. Then, the concentration of chloride ions decreased to approximately half (3.05 mg L^{-1}) after 6 h of treatment, which was in agreement with the results found by Mhemdi et al. [64] who studied the effect of the anode material (platinum and BDD) on the evolution of chlorides during the mineralization of 2-chlorobenzoic acid by an electrochemical oxidation process. The results showed that, for platinum, the concentration of chloride ions reached a maximum after 2 h and then remained constant. Using the BDD anode, a different behavior of chloride ions was observed. They accumulated rapidly after 1 h; then, their concentration decreased due to their oxidation to chlorine (Cl_2), which transformed into hypochlorite ions $HClO^-$ by hydrolysis. Consequently, the decrease in the accumulated chloride concentration during treatment could be explained by the oxidizing power of the BDD anode and the synthesized catalysts, causing the transformation of Cl^- ions into Cl_2.

Furthermore, the concentration of nitrate ions ($NO_3{}^-$) after 6 h was estimated at 0.68 mg L^{-1}. However, the accumulated concentration of ammonium ions ($NH_4{}^+$) was high, and it was around 4.75 mg L^{-1}. The accumulated concentrations of nitrate and ammonium ions after 6 h of treatment represent approximately 90% of the amount of nitrogen initially contained in the molecule of CDM. Consequently, one can confirm that CDM is mineralized during PEF application.

2.4. Stability of the Catalyst

2.4.1. Catalytic Stability

The recycling and reusability of a heterogeneous catalyst are important parameters for economic and environmental considerations [66]. The TOC abatement obtained using the same TiO_2/Fe_3O_4-CS(2) beads for four consecutive runs is depicted in Figure 4. After each run, the catalyst was washed with distilled water and dried at ambient temperature. The results showed that TOC removal remained almost constant for four cycles of reuse. The slight decrease (≃6.7%) observed in the fourth cycle could be attributed to the modification of the physicochemical properties of the catalyst's surface by the effect of UV-LED irradiation and the presence of H_2O_2 as an oxidant. In addition, possible leaching of Fe ions in the reaction medium was checked. The leached amount of Fe after each run did not exceed 1.7 mg L^{-1}, corresponding to 0.5% of the initial metal content in catalytic beads. These results revealed an excellent structural stability of the catalytic beads and minimal leaching of iron according to the environmental standards demanded by the European Union (<2 mg L^{-1}) [67].

2.4.2. Characterization of Catalyst before and after Use

SEM Analysis

The SEM images of TiO_2/Fe_3O_4-CS(2) beads before and after use are illustrated in Figure 5. As shown, the surface of the beads is smooth, indicating that iron and TiO_2 are attached to CS. The use of high magnification highlighted the observation of TiO_2 nanoparticles on the surface of the beads. The comparison of images in Figure 5a,b showed that, after four consecutive cycles, the surface of the beads was slightly damaged by oxidizing conditions and UV-LED irradiation, which explained the leaching of the metal.

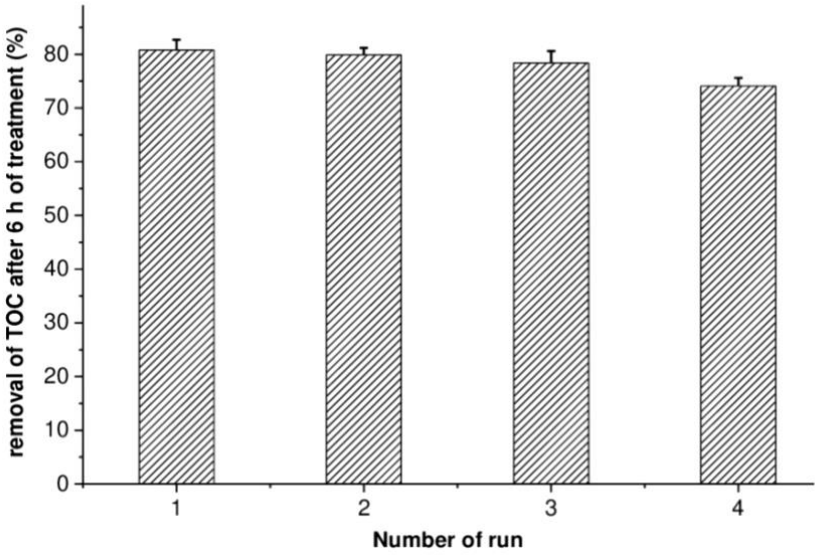

Figure 4. Stability of the catalytic activity of TiO_2/Fe_3O_4-CS(2) beads.

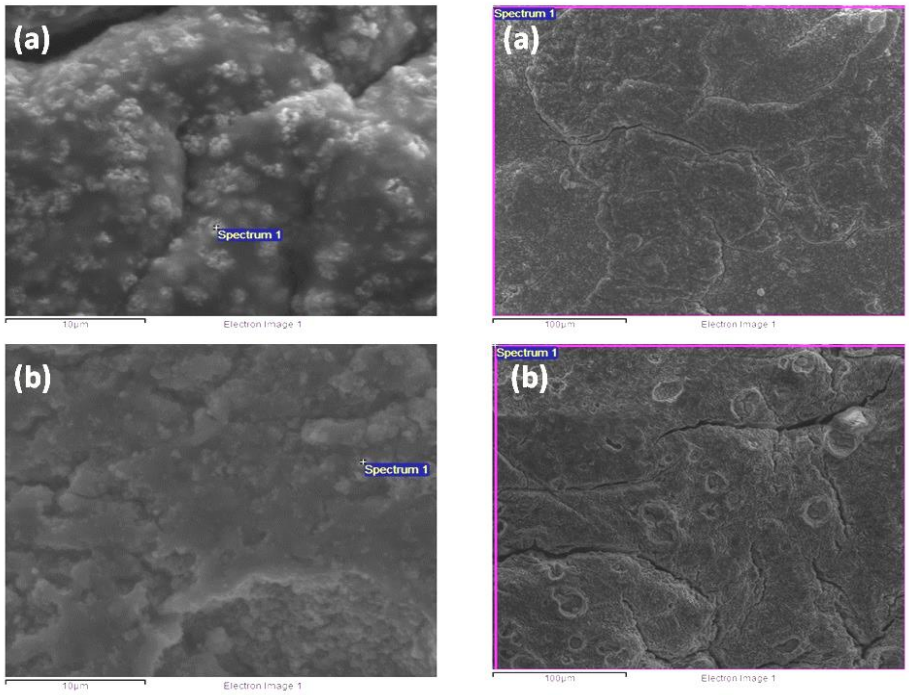

Figure 5. Morphology of catalyst: (**a**) TiO_2/Fe_3O_4-CS(2) before use, (**b**) TiO_2/Fe_3O_4-CS(2) after use.

XRD Analysis

In order to determine the crystalline structure of the TiO_2/Fe_3O_4-CS(2) beads, an XRD analysis was performed. In the XRD patterns (Figure 6a), the peak positions at 2Theta = 30.14°, 35.59°, 43.47°, 53.87°, 57.41° and 62.65° corresponded, respectively, to the Miller indices of (220), (311), (400), (422), (511) and (440) of the crystalline structure of Fe_3O_4, and the peak positions at 2Theta = 25.29°, 37.78°, 38.59°, 48.01°, 55.03°, 68.74°, 70,25°, 75.01°, 82.62° could be attributed to the diffraction planes of (110), (101), (004), (220), (105), (400), (220), (215) and (312) of the crystalline structure of TiO_2. The obtained peaks are well matched with standard data JCPDS-ICDD card N°:00-019-0629 for the Fe_3O_4 magnetite and 00-021-1272 for the TiO_2 anatase.

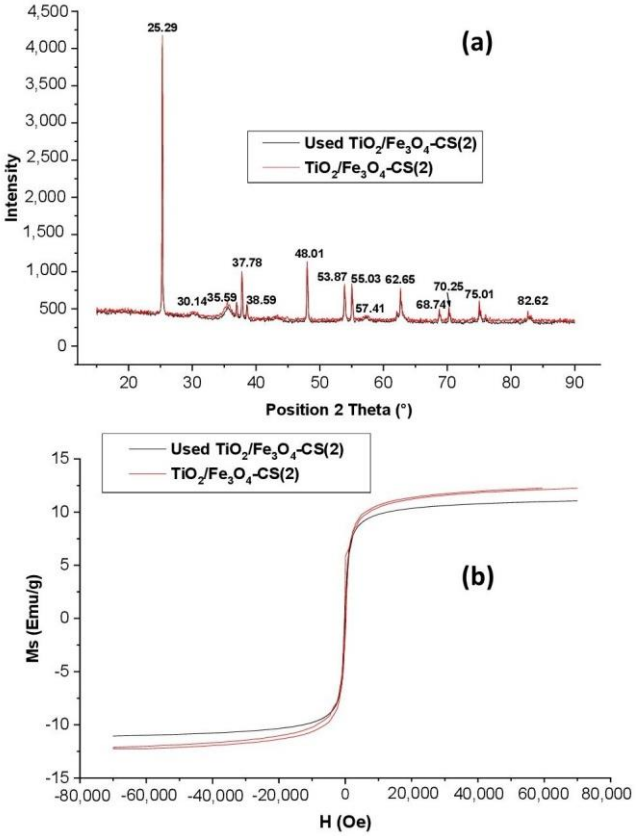

Figure 6. (**a**) X-ray diffraction patterns of TiO_2/Fe_3O_4-CS(2) beads, (**b**) Magnetization curves of the fresh and used TiO_2/Fe_3O_4-CS(2) beads.

The analysis of the catalytic beads used allowed us to obtain a diffractogram similar to that of fresh beads. In fact, indexing the pattern exhibited the crystal structure of the TiO_2 anatase (ICDD 00-021-1272). However, the peak positions at 2Theta = 30.14°, 35.59°, 43.47°, 48.01°, 55.03°, 57.41° and 62.65° corresponded, respectively, to the Miller indices of (220), (311), (400), (421), (422) (511) and (440) of the crystalline structure of maghemite Fe_2O_3 (ICDD 00-039-1346) instead of magnetite Fe_3O_4. Fe_2O_3 had the same spinel structure as magnetite, but it only contained iron in the trivalent Fe(III) state [68], which indicated the oxidation of Fe_3O_4. Furthermore, using the Debye–Scherrer equation, the grain size of TiO_2 was estimated at 64.5 nm, while the size of Fe_3O_4 was around 11.6 nm, indicating that the beads exhibit superparamagnetic behavior [69].

Magnetic Properties Analysis

The magnetization curve of the TiO_2/Fe_3O_4-CS(2) beads revealed a saturation intensity equal to 11.40 emu/g (Figure 6b). This low value is due to the presence of non-magnetic materials (CS and TiO_2) [70]. The magnetization intensity of the beads used was almost the same, and it was estimated at 10.48 emu g^{-1}, which means that the beads have a good stability of the magnetic properties after four consecutive cycles.

3. Materials and Methods

3.1. Chemical Products

All chemicals were of analytical–laboratory grade and applied without further purification. Chlordimeform, chitosan, sodium hydroxide, ferrous sulfate iron (II), iron (III) chloride, titanium oxide and potassium titanium oxide oxalate dehydrate were purchased from Sigma-Aldrich (Madrid, Spain). Acetic acid, sulfuric acid and nitric acid were supplied by Analar Normapur (Radnor, PA, USA). Acetonitrile (HPLC-grade) was purchased

from Fisher Scientific (Loughborough, UK). Ultrapure water obtained through reverse osmosis technology (Basic 360) was utilized throughout all the experiments.

3.2. Preparation of TiO_2/Fe_3O_4-Chitosan Magnetic Beads

An eco-friendly, low-cost and simple approach was used to synthesize the composite catalysts. Magnetic TiO_2/Fe_3O_4-CS beads were prepared via a precipitation method using sodium hydroxide (1 M) as a precipitating agent. First, 2% CS gel solution was prepared by dissolving 1 g of CS in acetic acid (1%) under stirring at room temperature. After the total dissolution of CS flakes, 5 mmol of iron salts at a molar ratio Fe^{3+}:Fe^{2+} = 2:1 was added. Then, the TiO_2 nanoparticles were blended in the iron salts–CS gel solution. The amount of TiO_2 varied from 5 mmol, 10 mmol to 15 mmol, which corresponds, respectively, to the molar ratios TiO_2/Fe equal to 1, 2 and 3. By adding TiO_2, the color of the solution changed from orange to white, as shown in Figure 7A. Then, the mixture was dropped through a syringe into the hardening sodium hydroxide solution to create spherical CS gel beads. The beads were washed several times with deionizer water to remove any residual alkali and dried in an oven at 50 °C.

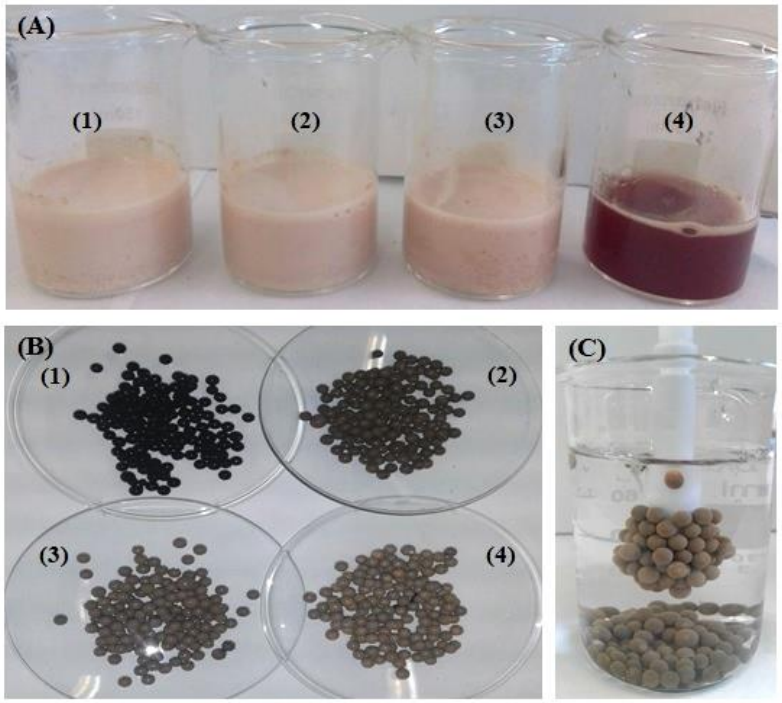

Figure 7. (**A**) Chitosan gel/Fe_3O solutions. (**B**) Wet chitosan beads ata molar ratio TiO_2/Fe: (**1**) 0; (**2**) 1; (**3**) 2 and (**4**) 3. (**C**) Superparamagnetic behavior of the TiO_{24}-CS beads ata molar ratio TiO_2/Fe = 2.

As seen in Figure 7B, the obtained beads are black for those containing iron only, and they take on a greenish coloration in the presence of TiO_2. All the prepared beads exhibited magnetic behavior in the presence of an external magnetic field (Figure 7C). The TiO_2-CS beads were prepared following the same alkaline co-precipitation method without addition of iron salts.

3.3. CDM Removal Assays

The PEF process of CDM degradation was performed in a cyclic mode, as shown in Figure 8. The process was composed of two reactors connected in series, allowing the treatment of (400 mL, 30 mgL^{-1}) CDM solution. A recirculation flow (200 mL min^{-1}) was set using a pump to connect the two reactors.

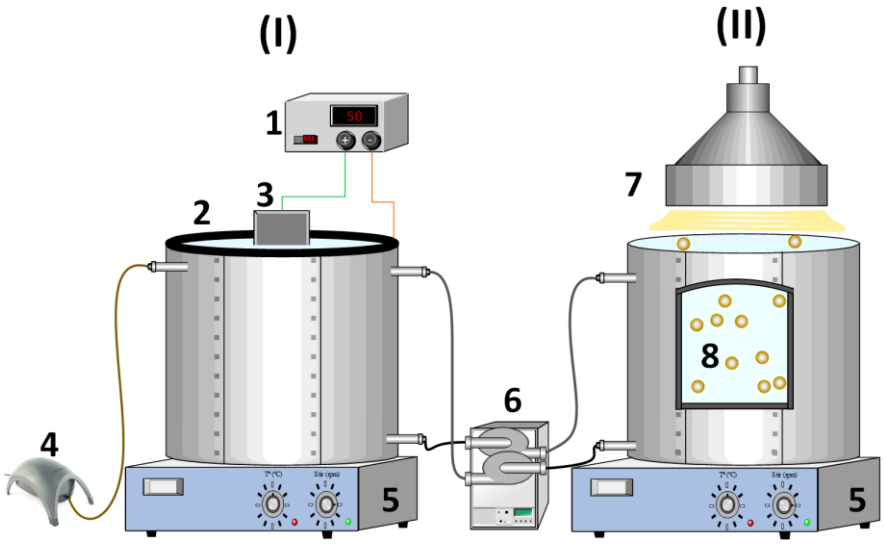

Figure 8. Cyclic electro-photocatalytic reactors: (**I**) electrochemical reactor: (**1**) power supply, (**2**) carbon felt electrode, (**3**) BDD electrode, (**4**) air supply, (**5**) magnetic stirrer, (**6**) peristaltic pump; (**II**) photocatalytic reactor: (**5**) magnetic stirrer, (**7**) UV-LED lamp, (**8**) catalytic beads.

The first reactor is electrochemical, composed of a glass beaker with a capacity of 250 mL, which permits the production of H_2O_2 by the reduction of dissolved oxygen on the cathode surface, which is a carbon felt (19.5 × 6 × 0.3 cm, Mersen, Barcelona, Spain) placed around the inner wall of the cylindrical cell, while the anode is a boron-doped diamond (BDD: 5 × 2.5 × 0.2 cm, Neocoat S.A.) placed in the middle of the cell. The system was run under a galvanostatic mode using an E 3512 A generator (Agilent, Santa Clara, CA, USA).

Na_2SO_4 was added previously as a support electrolyte at a concentration of 0.01 M, and the pH was adjusted to 3 using sulfuric acid solution. Air bubbling was maintained 15 min before the start of the reaction and through the treatment in order to saturate the medium with oxygen.

The second reactor is a cylindrical glass cell. A low-consumption UV-LED lamp (365 nm, 40 W, 550 lumens) from Luckylight electronics was placed above it, emitting at a wavelength equal to 365 nm. The catalyst was added into the photocatalytic reactor to promote its activation and avoid its electrochemical degradation, especially in the presence of a powerful oxidizing BDD anode in the first reactor.

To highlight the contribution of (photoelectrolysis + H_2O_2) and photocatalysis processes to the degradation of CDM, assays were conducted, respectively, without catalytic beads and in the absence of a current. Likewise, to evaluate the adsorption process contribution, another assay was conducted in the absence of UV irradiation and a current.

3.4. Analytical Methods

3.4.1. Determination of CDM Concentration

During experiments, the samples were collected and filtered prior to analysis through a 0.45 µm pore-size cellulose acetate membrane. CDM was quantified by HPLC (Agilent 1260 equipped with UV detector) with a C18 reverse-phase (4.6 mm × 250 mm, 5 µm; Agilent) column. The diode array detector was set at a fixed wavelength equal to 240 nm. The eluent was water/acetonitrile (60/40), with a flow rate of 1 mL min^{-1}.

3.4.2. Determination of Carboxylic Acids Concentrations

To identify and quantify the carboxylic acids generated during electrolysis, an HPLC was used with a diode array detector fixed at 206 nm. A Rezex™ ROA-Organic Acid H^+ (8%) (300 × 7.8 mm, i.e., 8 µm) column was used and placed in an oven at 60 °C. The eluent was 0.005 N H_2SO_4 solution pumped at a flow rate of 0.5 mL min^{-1}. The

identification of carboxylic acids was based on a comparison of the retention times with those of pure standards.

3.4.3. Determination of Ions Concentrations

The ions generated were quantitatively followed by an ion chromatography system DIONEX ICS-3000. The separation of ions was performed by a Metrosep A Supp 5 column (4.0 × 250 mm). The eluent was 3.2 mmol L^{-1} Na_2CO_3 and 1 mmol L^{-1} $NaHCO_3$ at a flow rate of 0.7 mL min^{-1}. The limit of quantification (LOQ) of all chromatographic methods was 0.1 mg L^{-1}.

3.4.4. Total Organic Carbon Measurements

The total organic carbon (TOC) was measured via catalytic high-temperature combustion by multi N/C 3100 equipment (Analytic Jena, Germany) coupled with a non-dispersive infrared detector. The percentage removal of TOC was calculated using the following equation:

$$\% \text{ removal of TOC} = \frac{TOC_0 - TOC_t}{TOC_0} \times 100 \quad (4)$$

with TOC_0 and TOC_t representing the initial TOC and that at instant t.

3.4.5. Determination of Fe Concentration

The Fe concentration was determined by Inductively Coupled Plasma ICP (model: Optima 4300 DV Perkin Elmer Instruments). To obtain a metal solution from the heterogeneous catalyst, an acid digestion method was carried out using a concentrated nitric acid solution with the beads and placed on an autoclave at 121°C (Danish standard DS250).

3.4.6. Determination of H_2O_2 Concentration

The concentration of H_2O_2 was determined by a colorimetric method using a (Thermo Electron Corporation Helios) spectrophotometer because a titanium oxalate complexing agent can react with H_2O_2, producing a yellow peroxo–titanium complex, which absorbs at λ_{max} = 400 nm [71].

3.4.7. Characterization of the Synthesized Catalysts

The surface morphology of the catalytic beads was observed using a scanning electron microscope (JEOL JSM-6700F). The crystalline structure of the obtained catalysts was determined by X-Ray Diffraction (XRD, X'Pert PRO MPD). Finally, the Physical Properties Measurement System equipment (PPMS Ever Cool-II 9T) with a Vibrating Sample Magnetometer (VSM) at 298 K was used to explore the magnetic properties of the catalysts.

3.5. Specific Energy Consumption

The electric energy consumption (EEC) per unit volume of treated solution (kWh m^{-3}) was calculated according to the following equation [72]:

$$EEC\left(\text{kWh m}^{-3}\right) = \frac{I \times E \times t}{V} \quad (5)$$

where I is the current applied (A), E is the average cell voltage (V), t is the electrolysis time (h), and V is the solution volume (L or m^3).

4. Conclusions

In summary, magnetic TiO_2/Fe_3O_4-CS beads were synthesized following an easy in situ co-precipitation approach. The molar ratio TiO_2/Fe was studied, and the enhanced catalytic activity of TiO_2/Fe_3O_4-CS, with a molar ratio equal to 2, was probably due to the reduced recombination of charge carriers on the surface of the catalyst.

The performance of the PEF process using TiO_2/Fe_3O_4-CS(2) as a photocatalyst for the treatment of real wastewater doped with CDM insecticide was evaluated under optimal

experimental conditions. Complete CDM removal was attained in 1 h, and more than 80% TOC abatement was achieved after 6 h of treatment, with simple carboxylic acids as the main by-product.

The catalytic activity of TiO_2/Fe_3O_4-CS(2) was satisfactorily validated in four consecutive cycles, and a slight decrease was obtained between the first and the fourth runs. Post-reaction catalyst characterization showed a high stability of magnetic properties despite the oxidation of Fe_3O_4 to Fe_2O_3, which is known for its good catalytic activity, sometimes similar to Fe_3O_4. Thus, the slight decrease in the catalytic activity could be attributed to the leaching of metals caused by the effect of the oxidizing conditions and UV-LED irradiation on catalytic beads.

This study offered a simple approach for constructing an eco-friendly, simple recovery and efficient bifunctional catalyst for advanced oxidation processes for treating recalcitrant organic pollutants in wastewater.

Author Contributions: Conceptualization, S.R.; Methodology, S.R. and A.M.D.; Validation, M.P. and M.Á.S.; Resources, M.P. and M.Á.S.; Writing—Original Draft Preparation, S.R.; Writing—Review and Editing, S.R., A.M.D., L.M., N.A., M.P. and M.Á.S.; Visualization, A.M.D., M.P. and M.Á.S.; Supervision, L.M., N.A., M.P. and M.Á.S.; Funding Acquisition, A.M.D., N.A., M.P. and M.Á.S. All authors have read and agreed to the published version of the manuscript.

Funding: This research was funded by Xunta de Galicia, grant number (ED481B 2019/091). This research was also funded by Project PID2020-113667GB-I00 464 funded by MCIN/AEI /10.13039/501100 011033. The authors are grateful to Xunta de Galicia for funding the researcher Aida Maria Díez Sarabia (ED481B 2019/091). This work was also financially supported by the Research Unit on Electrochemistry, Materials and Environment (UR16ES02) at the University of Kairouan in Tunisia.

Data Availability Statement: Data is contained within the article.

Conflicts of Interest: The authors declare no conflict of interest.

References

1. Malakootian, M.; Shahesmaeili, M.A.; Fraji, M.; Amiri, H.; Silva Martinez, S. Advanced oxidationprocesses for the removal of organophosphorus pesticides in aqueous matrices: A systematicreview and meta-analysis. *Process. Saf. Environ. Prot.* **2020**, *134*, 292–307. [CrossRef]
2. Torres, N.H.; de Oliveira Santiago Santos, G.; Ferreira, L.F.R.; Américo-Pinheiro, J.H.P.; Eguiluz, K.I.B.; Salazar-Banda, G.R. Environmental aspects of hormones estriol, 17β-estradiol and 17α-ethinylestradiol: Electrochemicalprocesses as next-generation technologies for theirremoval in water matrices. *Chemosphere* **2021**, *267*, 128888. [CrossRef] [PubMed]
3. Trellu, C.; Olvera Vargas, H.; Mousset, E.; Oturan, N.; Oturan, M.A. Electrochemical technologies for the treatment of pesticides. *Curr. Opin. Electrochem.* **2021**, *26*, 100677. [CrossRef]
4. Rajasekhar, B.; Venkateshwaran, U.; Durairaj, N.; Divyapriya, G.; Nambi, I.M.; Joseph, A. Comprehensivetreatment of urban-wastewatersusingelectrochemicaladvancedoxidation process. *J. Environ. Manag.* **2022**, *266*, 110469. [CrossRef] [PubMed]
5. Heidari, Z.; Pelalak, R.; Alizadeh, R.; Oturan, N.; Shirazian, S.; et Oturan, M.A. Application of Mineral Iron-Based Natural Catalysts in Electro-Fenton Process: A Comparative Study. *Catalysts* **2021**, *11*, 1–18. [CrossRef]
6. Ganzenko, O.; Trrellu, C.; Oturan, N.; Huguenot, D.; Péchaud, Y.; Van Hullebusch, E.D.; Oturan, M.A. Electro-Fenton treatment of a complex pharmaceutical mixture: Mineralization efficiency and biodegradability enhancement. *Chemosphere* **2020**, *253*, 126659. [CrossRef] [PubMed]
7. Hussain, S.; Aneggi, E.; et Goi, D. Catalytic activity of metals in heterogeneous Fenton-like oxidation of wastewater contaminants: A review. *Environ. Chem. Lett.* **2021**, *19*, 2405–2424. [CrossRef]
8. Guo, W.; Li, T.; Chen, Q.; Wan, J.; Zhang, J.; Wu, B.; Wang, Y. The roles of wavelength in the gaseous toluene removal with OH from UV activated Fenton reagent. *Chemosphere* **2021**, *275*, 129998. [CrossRef]
9. Babuponnusami, A.; Muthukumar, K. Advanced oxidation of phenol: A comparison between Fenton, electro-Fenton, sono-electro-Fenton and photo-electro-Fenton processes. *J. Chem. Eng.* **2012**, *183*, 1–9. [CrossRef]
10. Babuponnusami, A.; Muthukumar, K. Removal of phenol by heterogenous photo electro Fenton-like process using nano-zero valent iron. *Sep. Purif. Technol.* **2012**, *98*, 130–135. [CrossRef]
11. Chu, A.C.; Sahu, R.S.; Chou, T.H.; Shih, Y. Magnetic Fe_3O_4@TiO_2 nanocomposites to degrade bisphenol A, one emerging contaminant, under visible and long wavelength UV light irradiation. *J. Environ. Chem. Eng.* **2021**, *9*, 105539. [CrossRef]
12. Sun, Q.; Hong, Y.; Liu, Q.; Dong, L. Synergistic operation of photocatalytic degradation and Fenton process by magnetic Fe_3O_4 loaded TiO_2. *Appl. Surf. Sci.* **2018**, *430*, 399–406. [CrossRef]

13. Mukhtar, F.; Munawar, T.; Nadeem, M.S.; Rehman, M.N.; Khan, S.A.; Koc, M.; Batool, S.; Hasan, M.; Iqbal, F. Dual Z-scheme core-shell PANI-CeO_2-Fe_2O_3-NiO heterostructured nanocomposite for dyes remediation under sunlight and bacterial disinfection. *Environ. Res.* **2022**, *215*, 114140. [CrossRef] [PubMed]
14. Mukhtar, F.; Munawar, T.; Nadeem, M.S.; Khan, S.A.; Koc, M.; Batool, S.; Hasan, M.; Iqbal, F. Enhanced sunlight-absorption of Fe_2O_3 covered by PANI for the photodegradation of organic pollutants and antimicrobial inactivation. *Adv. Powder Technol.* **2022**, *33*, 103708. [CrossRef]
15. Goswami, A.; Jiang, J.-Q.; Petri, M. Treatability of five micro-pollutants using modified Fenton reaction catalyzed by zero-valent iron powder (Fe(0)). *J. Environ. Chem. Eng.* **2021**, *9*, 105393. [CrossRef]
16. Wang, Y.; Fang, J.; Crittenden, J.C.; Shen, C. Novel RGO/α-FeOOH supported catalyst for Fenton oxidation of phenol at a wide pH range using solar-light-driven irradiation. *J. Hazard. Mater.* **2017**, *239*, 321–329. [CrossRef]
17. Luo, H.; Zeng, Y.; He, D.; Pan, X. Application of iron-based materials in heterogeneous advanced oxidation processes for wastewater treatment: A review. *J. Chem. Eng.* **2021**, *407*, 127191. [CrossRef]
18. Dudchenko, N.; Pawar, S.; Perelshtein, I.; Fixler, D. Magnetite Nanoparticles: Synthesis and Applications in Optics and Nanophotonics. *Materials* **2022**, *15*, 2601. [CrossRef]
19. Nguyen, M.D.; Tran, H.-V.; Xu, S.; Lee, T.R. Fe_3O_4 Nanoparticles: Structures, Synthesis, Magnetic Properties, Surface Functionalization, and Emerging Applications. *Appl. Sci.* **2021**, *11*, 11301. [CrossRef]
20. Gopinath, K.P.; Madhav, V.M.; Krishnan, A.; Malolan, R.; Rangarajan, G. Present applications of titanium dioxide for the photocatalytic removal of pollutants from water: A review. *J. Environ. Manag.* **2020**, *270*, 110906. [CrossRef]
21. Mukhtar, F.; Munawar, T.; Nadeem, M.S.; Rehman, M.N.; Batool, S.; Hasan, M.; Riaz, M.; Rehman, K.; Iqbal, F. Highly efficient tri-phase TiO_2-Y_2O_3-V_2O_5 nanaocomposite: Structural, optical, photocatalyst and antibacterial studies. *J. Nanostruct. Chem.* **2022**, *12*, 547–564. [CrossRef]
22. Liu, C.; Dai, H.; Tan, C.; Pan, Q.; Hu, F.; Peng, X. Photo-Fenton degradation of tetracycline over Z-sheme Fe-g-C_3N_4/Bi_2WO_6 heterojunctions: Mechanism insight, degradation pathways and DFT calculation. *Appl. Catal. B* **2022**, *310*, 121326. [CrossRef]
23. Sun, L.; Zhou, Q.; Mao, J.; Ouyang, X.; Yuan, Z.; Song, X.; Gong, W.; Mei, S.; Xu, W. Study on Photocatalytic Degradation of Acid Red 73 by Fe_3O_4@TiO_2 Exposed (001) Facets. *Appl. Sci.* **2022**, *12*, 3574. [CrossRef]
24. Rezgui, S.; Díez, A.M.; Monser, L.; Adhoum, N.; Pazos, M.; et Sanromán, M.A. $ZnFe_2O_4$-chitosan magnetic beads for the removal of chlordimeform by photo-Fenton process under UVC irradiation. *J. Environ. Manag.* **2021**, *283*, 111987. [CrossRef] [PubMed]
25. Rezgui, S.; Amrane, A.; Fourcade, F.; Assadi, A.; Monser, L.; Adhoum, N. Electro-Fenton catalyzed with magnetic chitosan beads for the removal of Chlordimeform insecticide. *Appl. Catal. B* **2018**, *226*, 346–359. [CrossRef]
26. Lee, M.; Chen, B.-Y.; Den., W. Chitosan as a Natural Polymer for Heterogeneous Catalysts Support: A. Short Review on Its Applications. *Appl. Sci.* **2015**, *5*, 1272–1283. [CrossRef]
27. Zhang, W.; Jia, S.; Wu, Q.; Wu, S.; Ran, J.; Lui, Y.; Hou, J. Studies of the magnetic field intensity on the synthesis of chitosan-coated magnetite nanocomposites by co-precipitation method. *Mater. Sci. Eng. C* **2012**, *32*, 381–384. [CrossRef]
28. Donadel, K.; Felisberto, M.D.V.; Fávere, V.T.; Rigoni, M.; Batistela, N.J.; Laranjeira, C.M.C. Synthesis and characterization of the iron oxide magnetic particles coated with chitosan biopolymer. *Mater. Sci. Eng. C* **2008**, *28*, 509–514. [CrossRef]
29. Moura, F.C.C.; Araujo, M.H.; Costa, R.C.C.; Ardisson, J.D.; Macedo, W.A.A.; Lago, R.M. Efficient use of Fe metal as an electron transfer agent in a heterogeneous Fenton system based on Fe^0/Fe_3O_4 composites. *Chemosphere* **2005**, *60*, 1118–1123. [CrossRef]
30. Sun, Q.; Leng, W.; Li, Z.; Xu, Y. Effect of surface Fe_2O_3 clusters on the photocatalytic activity of TiO_2 for phenol degradation in water. *J. Hazard. Mater.* **2012**, *229–230*, 224–232. [CrossRef]
31. Afzal, S.; Julkapli, N.M.; Mun, L.K. Visible light active TiO_2/CS/Fe_3O_4 for nitrophenol degradation: Studying impact of TiO_2, CS and Fe_3O_4 loading on the optical and photocatalytic performance of nanocomposite. *Mater. Sci. Semicond. Process.* **2021**, *131*, 105891. [CrossRef]
32. Díez, A.M.; Pazos, M.; Sanromán, M.A. Synthesis of magnetic-photo-Fenton catalyst for degradation of emerging pollutant. *Catal. Today* **2019**, *328*, 267–273. [CrossRef]
33. Li, Y.; Cheng, H. Chemical kinetic modeling of organic pollutant degradation in Fenton and solar photo-Fenton processes. *J. Taiwan Inst. Chem. Eng.* **2021**, *123*, 175–184. [CrossRef]
34. Burbano, A.A.; Dionysiou, D.D.; Suidan, M.T.; Richardson, T.L. Oxidation kinetics and effect of pH on the degradation of MTBE with Fenton reagent. *Water Res.* **2016**, *39*, 107–118. [CrossRef] [PubMed]
35. Molamahmood, H.V.; Geng, W.; Wei, Y.; Miao, J.; Yu, S.; Shahi, A.; Chen, C.; Long, M. Catalyzed H_2O_2 decomposition over iron oxides and oxyhydroxides: Insights from oxygen production and organic degradation. *Chemosphere* **2022**, *291*, 133037. [CrossRef]
36. Li, Q.; Kong, H.; Jia, R.; Shao, J.; He, Y. Enhanced catalytic degradation of amoxicillin with TiO_2–Fe_3O_4 composites via a submerged magnetic separation membrane photocatalytic reactor (SMSMPR). *RSC Adv.* **2019**, *9*, 12538–12546. [CrossRef]
37. Li, Q.; Kong, H.; Li, P.; Shao, J.; He, Y. Photo-Fenton degradation of amoxicillin via magnetic TiO_2-graphene oxide-Fe_3O_4 composite with a submerged magnetic separation membrane photocatalytic reactor (SMSMPR). *J. Hazard. Mater.* **2019**, *373*, 437–446. [CrossRef]
38. Bai, X.; Lyu, L.; Ma, W.; Ye, Z. Heterogeneous UV/Fenton degradation of bisphenol A catalyzed by synergistic effects of $FeCo_2O_4$/TiO_2/GO. *Environ. Sci. Pollut. Res.* **2016**, *23*, 22734–22743. [CrossRef]
39. Nwe, T.S.; Sikong, L.; Kokoo, R.; Khangkhamano, M. Photocatalytic activity enhancement of Dy-doped TiO_2 nanoparticles hybrid with TiO_2 (B) nanobelts under UV and fluorescence irradiation. *Curr. Appl. Phys.* **2016**, *20*, 249–254. [CrossRef]

40. Nam, Y.; Lim, J.H.; Ko, K.C.; Lee, J.K. Photocatalytic activity of TiO_2 nanoparticles: A theoretical aspect. *J. Mater. Chem. A* **2019**, *7*, 13833–13859. [CrossRef]
41. Enesca, A.; Isac, L. The Influence of Light Irradiation on the Photocatalytic Degradation of Organic Pollutants. *Materials* **2020**, *11*, 2494. [CrossRef] [PubMed]
42. Boruah, P.K.; Das, M.R. Dual responsive magnetic Fe_3O_4-TiO_2/graphene nanocomposite as an artificial nanozymes for the colorimetric detection and photodegradation of pesticide in an aqueous medium. *J. Hazard. Mater.* **2020**, *385*, 121516. [CrossRef] [PubMed]
43. Pourzad, A.; Sobhi, H.R.; Behbahani, M.; Esrafili, A.; Kalantary, R.R.; Kermani, M. Efficient visible light-induced photocatalytic removal of paraquat using N-doped TiO_2@SiO_2@Fe_3O_4 nanocomposite. *J. Mol. Liq.* **2020**, *299*, 112467. [CrossRef]
44. Zahedifar, M.; Seyedi, N. Bare 3D-TiO_2/magnetic biochar dots (3D-TiO_2/BCDs MNPs): Highly efficient recyclable photocatalyst for diazinon degradation under sunlight irradiation. *Phys. E Low-Dimens. Syst. Nanostruct.* **2022**, *139*, 115151. [CrossRef]
45. Hua, Y.; Wang, S.; Xiao, J.; Cui, C.; Wang, C. Preparation and characterization of Fe_3O_4/gallic acid/graphene oxide magnetic nanocomposites as highly efficient Fenton catalysts. *RSC Adv.* **2017**, *7*, 28979–28986. [CrossRef]
46. Kasiri, M.B.; Aleboyeh, H.; Aleboyeh, A. Degradation of Acid Blue 74 using Fe-ZSM5 zeolite as a heterogeneous photo-Fenton catalyst. *Appl. Catal. B* **2008**, *84*, 9–15. [CrossRef]
47. Tekbaş, M.; Yatmaz, H.C.; Bektaş, N. Heterogeneous photo-Fenton oxidation of reactive azo dye solutions using iron exchanged zeolite as a catalyst. *Microporous Mesoporous Mater.* **2008**, *115*, 594–602. [CrossRef]
48. Jiang, B.; Niu, Q.; Li, C.; Oturan, N.; Oturan, M.A. Outstanding performance of electro-Fenton process for efficient decontamination of Cr(III) complexes via alkaline precipitation with no accumulation of Cr(VI): Important roles of iron species. *Appl. Catal. B* **2020**, *272*, 119002. [CrossRef]
49. Hammouda, S.B.; Amrane, A.; Fourcade, F.; Assadi, A.; Adhoum, N.; Monser, L. Effective heterogeneous electro-Fenton process for the degradation of a malodorous compound indole using iron loaded alginate beads as a reusable catalyst. *Appl. Catal. B* **2016**, *182*, 47–58. [CrossRef]
50. Liu, D.; Zhang, H.; Wei, Y.; Liu, B.; Lin, Y.; Li, G.; Zhang, F. Enhanced degradation of ibuprofen by heterogeneous electro-Fenton at circumneutral pH. *Chemosphere* **2018**, *209*, 998–1006. [CrossRef]
51. Chmayssem, A.; Taha, S.; Hauchard, D. Scaled-up electrochemical reactor with a fixed bed three-dimensional cathode for electro-Fenton process: Application to the treatment of bisphenol A. *Electrochim. Acta* **2017**, *225*, 435–442. [CrossRef]
52. Nidheesh, P.V.; Gandhimathi, R. Trends in electro-Fenton process for water and wastewater treatment: An overview. *Desalination* **2012**, *299*, 1–15. [CrossRef]
53. Kang, B.; Dai, Y.; Zhang, H.; Chen, D. Synergetic degradation of chitosan with gamma radiation and hydrogen peroxide. *Polym. Degrad. Stab.* **2007**, *92*, 359–362. [CrossRef]
54. Wang, S.-M.; Huang, Q.-Z.; Wang, Q.-S. Study on the synergetic degradation of chitosan with ultraviolet light and hydrogen peroxide. *Carbohydr. Res.* **2005**, *340*, 1143–1147. [CrossRef]
55. Zazouli, M.A.; Ghanbari, F.; Yousefi, M.; Madihi-Bidgoli, S. Photocatalytic degradation of food dye by Fe_3O_4–TiO_2 nanoparticles in presence of peroxymonosulfate: The effect of UV sources. *J. Environ. Chem. Eng.* **2017**, *5*, 2459–2468. [CrossRef]
56. Maktabifard, M.; Zaborowska, E.; Makinia, J. Achieving energy neutrality in wastewater treatment plants through energy savings and enhancing renewable energy production. *Rev. Environ. Sci. Biotechnol.* **2018**, *17*, 655–689. [CrossRef]
57. Ghazouani, M.; Bousselmi, L.; Akrout, H. Combined electrocoagulation and electrochemical treatment on BDD electrodes for simultaneous removal of nitrates and phosphates. *J. Environ. Chem. Eng.* **2020**, *8*, 104509. [CrossRef]
58. Ghanbari, F.; Moradi, M.A. comparative study of electrocoagulation, electrochemical Fenton, electro-Fenton and peroxi-coagulation for decolorization of real textile wastewater: Electrical energy consumption and biodegradability improvement. *J. Environ. Chem. Eng.* **2015**, *3*, 499–506. [CrossRef]
59. Gerek, E.E.; Yılmaz, S.; Koparal, A.S.; Gerek, Ö.N. Combined energy and removal efficiency of electrochemical wastewater treatment for leather industry. *J. Water Process. Eng.* **2019**, *30*, 100382. [CrossRef]
60. Flores, N.; Sirés, I.; Garrido, J.A.; Centellas, F.; Rodriguez, R.M.; Cabot, P.L.; Brillas., E. Degradation of trans-ferulic acid in acidic aqueous medium by anodic oxidation, electro-Fenton and photoelectro-Fenton. *J. Hazard. Mater.* **2016**, *319*, 3–12. [CrossRef]
61. Hammami, S.; Oturan, N.; Bellakhal, N.; Dachraoui, M.; Oturan, M.A. Oxidative degradation of direct orange 61 by electro-Fenton process using a carbon felt electrode: Application of the experimental design methodology. *J. Electroanal. Chem.* **2007**, *610*, 75–84. [CrossRef]
62. Aplin, R.; Feitz, A.J.; Waite, T.D. Effect of Fe(III)-ligand properties on effectiveness of modified photo-Fenton processes. *Water Sci. Technol.* **2001**, *44*, 23–30. [CrossRef] [PubMed]
63. Zazou, H.; Oturan, N.; Zhang, H.; Hamdani, M.; Oturan, M.A. Comparative study of electrochemical oxidation of herbicide 2,4,5-T: Kinetics, parametric optimization and mineralization pathway. *Sustain. Environ. Res.* **2017**, *27*, 15–23. [CrossRef]
64. Mhemdi, A.; Oturan, M.A.; Oturan, N.; Abdelhédi, R.; Ammar, S. Electrochemical advanced oxidation of 2-chlorobenzoic acid using BDD or Pt anode and carbon felt cathode. *J. Electroanal. Chem.* **2013**, *709*, 111–117. [CrossRef]
65. Skoumal, M.; Arias, C.; Cabot, P.L.; Centellas, F.; Garrido, J.A.; Rodriguez, R.M.; Brillas, E. Mineralization of the biocide chloroxylenol by electrochemical advanced oxidation processes. *Chemosphere* **2008**, *71*, 1718–1729. [CrossRef]
66. Arai, M.; Zhao, F. Metal Catalysts Recycling and Heterogeneous/Homogeneous Catalysis. *Catalysts* **2015**, *5*, 868–870. [CrossRef]

67. Thomas, N.; Dionysiou, D.D.; Pillai, S.C. Heterogeneous Fenton catalysts: A review of recent advances. *J. Hazard. Mater.* **2021**, *404*, 124082. [CrossRef]
68. Rusevova, K.; Kopinke, F.-D.; Georgi, A. Nano-sized magnetic iron oxides as catalysts for heterogeneous Fenton-like reactions—Influence of Fe(II)/Fe(III) ratio on catalytic performance. *J. Hazard. Mater.* **2012**, *241–242*, 433–440. [CrossRef]
69. Gijs, M.A.M. Magnetic bead handling on-chip: New opportunities for analytical applications. *Microfluid. Nanofluid.* **2004**, *1*, 22–40. [CrossRef]
70. Li, Y.; Zhang, M.; Guo, M.; Wang, X. Preparation and properties of a nano TiO_2/Fe_3O_4 composite superparamagnetic photocatalyst. *Rare Metals* **2009**, *28*, 423–427. [CrossRef]
71. Almuaibed, A.M.; Townshend, A. Flow spectrophotometric method for determination of hydrogen peroxide using a cation exchanger for preconcentration. *Anal. Chim. Acta* **1994**, *295*, 159–163. [CrossRef]
72. Martínez-Huitle, C.A.; Brillas, E. Decontamination of wastewaters containing synthetic organic dyes by electrochemical methods: A general review. *Appl. Catal. B* **2009**, *87*, 105–145. [CrossRef]